ChemComm

COMMUNICATION

View Article Online
View Journal

Cite this: DOI: 10.1039/d6cc02132h

Received 8th April 2026,
Accepted 18th May 2026

DOI: 10.1039/d6cc02132h

rsc.li/chemcomm

Imaging the reactivity of carbon nitride nanosheets by photoinduced cathodic electrochemiluminescence microscopy

Chuan Li,[ab] Wei Zhang,*[ab] Changlin Zhou,[b] Fatima Merhi,[b] Bertrand Goudeau,[b] Patrick Garrigue,[b] Gabriel Loget*[b] and Neso Sojic*[b]

Carbon nitride (CN) is a highly promising electrochemiluminescence (ECL) nanomaterial operating in aqueous media at physiological pH. Here, we report the upconversion photoinduced ECL (PECL) emission on a p-type Si modified with CN nanosheet (p-Si/CNNS) photocathode in aqueous solution. The PECL activity of the single micrometer-sized CNNS was directly imaged by microscopy, revealing the heterogeneity at the single-particle level. In addition, the reported approach allows decreasing the onset ECL potential to −0.47 V *vs.* Ag/AgCl. This study opens new avenues for light-addressable electrochemical systems, the optimization of CNNS reactivity, and the study of new ECL materials.

Due to the advantages of fast-response, electrochemical control and high sensitivity, electrochemiluminescence (ECL) in aqueous electrolytes at physiological pH has become widely used for sensing[1–6] in the field of medical diagnosis. The traditional ECL approach measures averaged luminescence originating from a large ensemble of individual luminophores, while ECL microscopy[7–10] allows single-entity imaging[11,12] from single particles to single (bio)molecules.[13–16] In cathodic ECL, most of the luminophores, especially carbon-based nanomaterials[17–21] such as graphene quantum dots[22,23] and carbon dots,[24,25] were well recognized to emit strong ECL at a more negative potential than −1.2 V (all potentials are referred against Ag/AgCl, 3 M KCl) with persulfate, the typical cathodic coreactant. Since its first report in 2012,[26] graphitic carbon nitride (CN)[27–30] has become a highly promising cathodic ECL luminophore due to excellent conductive catalytic properties, large specific surface area,[29] low toxicity and tunable luminescence characteristics. With this system, the ECL emission onset, controlled by electron injection in the conduction band of CN, usually starts at −0.82 V and requires a negative cathodic potential (over −0.9 V)[31] to reach an important output signal. Many chemical modification methods such as heteroatom doping, defect introduction[31] and heterostructuration[32] were performed on CN to lower the trigger potential. Li *et al.*[33] designed nickel single-atom doped CN and reported nitrogen vacancy engineering of nickel single-atom catalyst CN, which slightly shifted the onset potentials to −0.80 and −0.72 V, respectively. Liu *et al.*[34] developed potassium doped CN, which achieved a large shift of the ECL excitation peak potential from −1.56 to −0.73 V with an onset potential of around −0.5 V and a red-shifted emission.

Photoinduced electrochemiluminescence (PECL) is a growing field of research that combines semiconductor (SC) photoelectrochemistry and ECL.[35–46] Compared with conventional ECL, upon illumination of the SC photoelectrode, interfacial charge transfer with photogenerated minority carriers enables ECL emission at lower applied potentials due to photovoltage generation, thereby improving biocompatibility. PECL also enables near IR imaging[47] and the construction of direct light-addressable[48] devices.[49] In contrast to photoluminescence (PL), this photoexcitation–ECL decoupling mechanism intrinsically suppresses both optical scattering and sample autofluorescence, thereby markedly enhancing the signal-to-noise ratio and spatial resolution. It should be pointed out that a major challenge for PECL is the poor stability of the SC photoelectrodes, which are prone to corrosion upon exposure to air and an aqueous electrolyte. To date, aqueous PECL has only been demonstrated using photoanodes with specific luminophores (luminol, L-012,[50] and $[Ru(bpy)_3]^{2+}$). These systems employed stabilized photoanodes, such as (n-type Si) n-Si-based materials protected with transition metal thin films[51,52] and stable oxide-based SC photoanodes.[41] Moreover, PECL images of single cells[42] and electrocatalysts have been recorded. As an alternative to anodic PECL, the less-explored cathodic PECL based on p-type SCs is expected to benefit stability, as detrimental surface oxidation is inhibited on negatively polarized Si-based electrodes.[53–55] So far, PECL on photocathodes has only been proposed in organic solvents with a diphenylanthracene

[a] School of Chemistry and Chemical Engineering, Liaocheng University, Liaocheng, Shandong, 252059, China. E-mail: weizhanglc@163.com
[b] Univ. Bordeaux, CNRS UMR 5255, Bordeaux INP, Site ENSMAC, 33607, Pessac, France. E-mail: gabriel.loget@cnrs.fr, sojic@u-bordeaux.fr

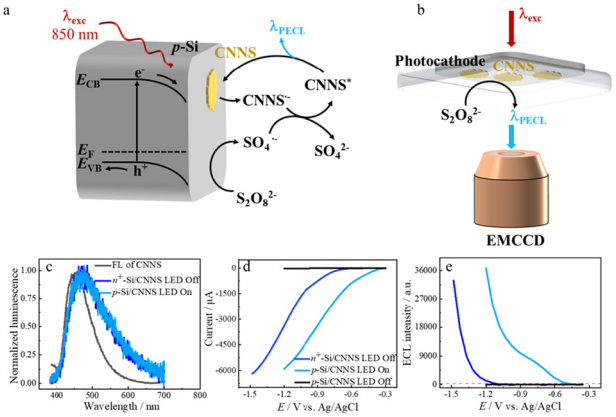

Fig. 1 (a) Scheme of a p-Si/CNNS photocathode during the photoinduced ECL process under near IR irradiation (λ_{exc} = 850 nm). E_f, E_{CB} and E_{VB} represent the Fermi level, conduction band and valence band of p-Si, respectively. (b) Scheme of the PECL microscopy setup. (c) Fluorescence (FL) spectrum of CNNS in absolute ethanol (black, excitation at 365 nm), ECL spectrum recorded on n^+-Si/CNNS in the dark (dark blue) and PECL spectrum recorded under near IR illumination on p-Si/CNNS (cyan). (d) Linear sweep voltammograms recorded under near IR irradiation on p-Si/CNNS (cyan), in the dark on n^+-Si/CNNS (dark blue) and on p-Si/CNNS (black). (e) Corresponding ECL intensity profiles. Measurements were performed in 0.1 M PBS with 0.1 M $K_2S_2O_8$. Scan rate: 50 mV s^{-1}.

derivative *via* an ion-annihilation pathway[56,57] and $[Ru(bpy)_3]^{2+}$/benzoyl peroxide *via* a cathodic ECL pathway.[58]

Here, we report an upconversion PECL system operating in aqueous solution (pH 7.4), using a p-Si modified with CN nanosheet (CNNS) photocathode (p-Si/CNNS). For an unmodified CNNS, the PECL onset potential achieved an unprecedentedly low potential (−0.47 V). The ability of PECL to trigger ECL at low potentials was first validated on a cathodic solid-state luminophore. In addition, clear and dynamic PECL images of single CNNS particles were observed, for the first time, at −0.9 V, showing the reactivity map of the material.

In our experiment, the CNNS particles were directly immobilized on p-Si. As depicted in Fig. 1a and b, the upconversion PECL of the p-Si/CNNS photocathode was studied with $K_2S_2O_8$ as a coreactant, in PBS at pH 7.4. The photocathodes were prepared as follows: a suspension of CNNS in absolute ethanol was dropped onto freshly hydrogenated p-Si electrodes and dried at room temperature. Under illumination (850 nm), electrons photogenerated inside or close to the p-Si depletion region can participate in the electrochemical reactions if the downward band bending (*i.e.*, the applied potential) is sufficiently large. At the p-Si/electrolyte interface, electrons reduce $S_2O_8^{2-}$ to a strongly reactive radical $SO_4^{\bullet-}$ and CNNS to $CNNS^{\bullet-}$. $SO_4^{\bullet-}$ oxidizes $CNNS^{\bullet-}$, leading to its excited state CNNS* (Fig. 1a). The excited luminophore returns to the ground state by emitting a photon at λ_{ECL} = 468 nm (Fig. 1c, cyan curve), consistent with previous works.[26] As a control experiment, the ECL of CNNS on a heavily doped non-photoactive n^+-Si/CNNS electrode (essentially behaving as a conductor) was also studied in the dark. The ECL spectrum of p-Si/CNNS well overlapped with that of n^+-Si/CNNS (Fig. 1c, blue curve), and both were red-shifted by 13 nm compared with the fluorescence emission band at 455 nm (Fig. 1c, dark curve) of CNNS in absolute ethanol. During our experiments, all voltammograms and PECL experiments were recorded in 0.1 M PBS with 0.1 M $K_2S_2O_8$.

The p-Si/CNNS photocathodes were first studied by linear sweep voltammetry (LSV) from −0.3 to −1.2 V under near IR irradiation and in the dark. The LSV curve in Fig. 1d shows that no current was observed in the dark (black curve); however, a photocurrent started to increase significantly from −0.31 V under illumination, which is attributed to the reduction of $S_2O_8^{2-}$ on the p-Si surface. This is demonstrated by the LSV curve recorded without $S_2O_8^{2-}$ (Fig. S1a). The current recorded for n^+-Si/CNNS in the dark (Fig. 1d) starts to increase significantly from −0.62 V. The corresponding ECL intensity plots, shown in Fig. 1e, reveal no ECL response from p-Si/CNNS in the dark and an onset of PECL emission at −0.47 V, which increased considerably until −1.2 V under illumination. The ECL was attributed to the excited CNNS* produced by the exergonic reaction between $CNNS^{\bullet-}$ and $SO_4^{\bullet-}$ in close proximity to the p-Si electrode (this is in good agreement with the ECL experiments performed on p-Si/CNNS in the absence of $S_2O_8^{2-}$, Fig. S1b). Under the same conditions, the onset of ECL emission was observed at −1.1 V for n^+-Si/CNNS in the dark (Fig. 1e). Fig. 2 shows the ECL spectra collected on both n^+-Si/CNNS in the dark (left) and p-Si/CNNS under illumination (right) during the LSV measurements recorded from −0.3 V to −1.2 V. A significant positive shift (+630 mV) of the emission onset potential was found for p-Si/CNNS under illumination compared with that recorded for n^+-Si/CNNS in the dark (Fig. S2). The underlying mechanism is elaborated in Section S2.1 of the SI.

The composition of the outermost surface of the electrodes was analyzed by X-ray photoelectron spectroscopy (XPS; Fig. S3a). The spectrum recorded for bare p-Si indicates that, before CNNS deposition, the surface consists only of Si and O atoms, with a low content of adventitious C, N and F. The spectrum acquired from the region containing CNNS confirms the presence of the deposited CNNS, as evidenced by significantly enhanced C 1s and N 1s peaks. These spectra also feature a strong decrease in the Si 2p and O 1s peak intensities. The high-resolution XPS spectra (Fig. S3b–d) are discussed in Section S2.3 of the SI. AFM (Fig. S4) and low-resolution (Fig. S5) and high-resolution scanning electron microscopy (SEM;

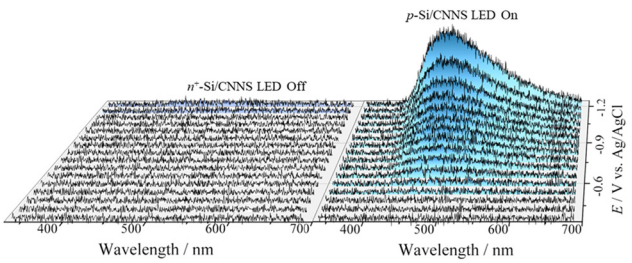

Fig. 2 Emission spectra recorded from −0.3 to −1.2 V in the dark on n^+-Si/CNNS (blue) and under near IR illumination on p-Si/CNNS (cyan). The measurements were performed in 0.1 M PBS with 0.1 M $K_2S_2O_8$. Scan rate: 50 mV s^{-1}.

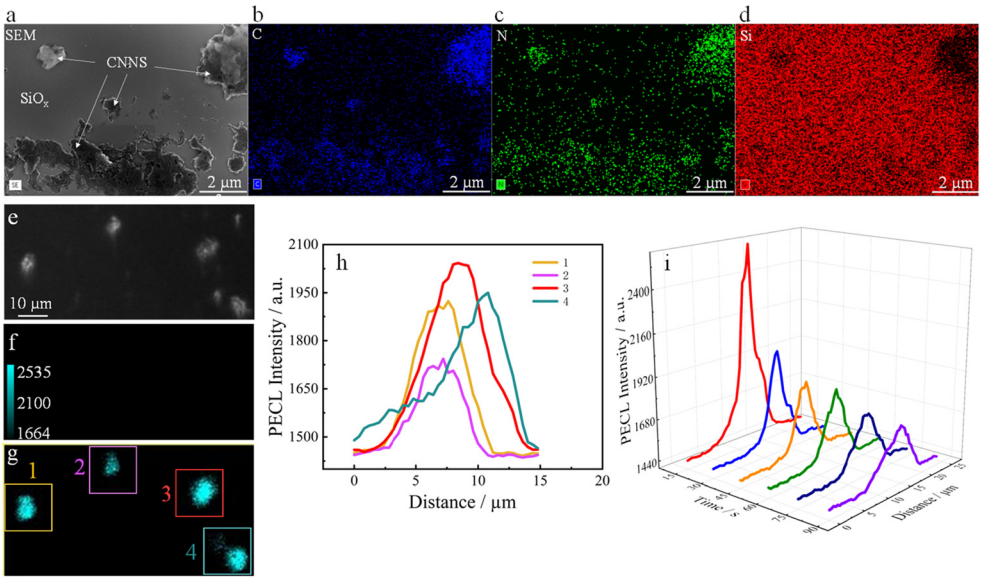

Fig. 3 (a) SEM images of CNNS deposited on p-Si and EDS mapping of C (b, blue), N (c, green) and Si (d, red). (e)–(i) Microscopy images of individual CNNS on p-Si/CNNS. Darkfield image (e) and corresponding PECL images in the dark (f) and (g) under 850 nm irradiation at −0.9 V. (h) PECL intensity profiles extracted for the four CNNS particles selected on p-Si/CNNS (see panel (g)). (i) Variation of PECL intensity profiles of the selected CNNS #3 as a function of time. Electrolyte: 0.1 M PBS with 0.1 M $K_2S_2O_8$.

Fig. 3a) were performed on the as-prepared p-Si/CNNS surfaces and revealed CNNS particles with a size distribution ranging from 0.1 to 7 μm with a height of ∼250 nm for the largest CNNS particles (Fig. S4b). EDS mapping (Fig. 3b–d) revealed that C and N were well distributed within the CNNS particles, whereas a weaker Si signal was observed in regions with thick CNNS coverage. EDS elemental analysis of selected regions of p-Si/CNNS (Fig. S6) is discussed in Section S2.5. PECL imaging was performed at a constant potential of −0.9 V under illumination with the largest CNNS particles, as depicted in Fig. 1b (see Sections S1.2 and S1.6). The corresponding current–time curves were recorded and are shown in Fig. S7. Four well-defined CNNS particles' surfaces were selected based on the dark field image (Fig. 3e). The PECL profiles (Fig. 3h) of these four CNNS particles are indicated by the colored solid squares in Fig. 3g. Their physical size was first estimated from the images obtained in dark field mode, and the full widths at half maximum were 3.5, 2.8, 6.0, and 4.2 μm. For the same CNNS particles, the full widths at half maximum were also extracted from the PECL images, yielding the following values: 4.8, 4.3, 5.4, and 5.3 μm, respectively. The enlarged apparent dimensions of CNNS particles in PECL mode might be related to the fact that even thin edges of the CNNS particles emit PECL light, whereas they are more difficult to image in the dark field mode. The emitted PECL light is stronger in the centre than at the edges, and some inhomogeneities could be observed. However, this may be related to the particles' thickness and the contact between the CNNS particles and the electrode. As a control, PECL imaging was performed under identical conditions on (i) p-Si/CNNS in an electrolyte lacking $K_2S_2O_8$ and (ii) bare p-Si; no ECL emission was detected in either case. In addition, the temporal evolution of the PECL signal was measured on the four selected CNNS particles by analyzing sequential PECL images (Fig. S8a–f). It was clearly visible that the four CNNS particles appeared when the light (λ_{exc} = 850 nm) was switched on and then PECL intensity exhibited a gradual decrease and subsequently stabilized at a plateau. The PECL profile of CNNS #3 as a function of time is shown in Fig. 3i, which clearly shows a progressive decrease over time until reaching a quasi-stable intensity. The reasons for the attenuation of luminous intensity are discussed in Section S2.7 of the SI.

To conclude, we exploited upconversion PECL to trigger the emission of CNNS deposited on photoactive p-Si at an unprecedentedly low potential without any chemical modification of the nanomaterials. Single CNNS particles were imaged by PECL microscopy. The reported approach enables spatiotemporal resolution of CNNS particles' emission, which reflects their local reactivity. In addition, the potential required to generate strong ECL emission was notably reduced to −0.47 V under physiological conditions. The PECL approach has great potential to be extended to other cathodic carbon-based materials. Finally, PECL microscopy opens new opportunities for imaging the reactivity of single photoactive nanoparticles and catalytic nanomaterials.

Conflicts of interest

There are no conflicts to declare.

Data availability

The data supporting this article have been included as part of the supplementary information (SI). Supplementary information is available. See DOI: https://doi.org/10.1039/d6cc02132h.

Acknowledgements

This work was financially supported by the Natural Science Foundation of Shandong Province (ZR2021QB080), the National Natural Science Foundation of China (21804063), and the French National Research Agency as a part of the France 2030 Program, under grant ANR-24-EXLU-3400014 (project VISIBLE of PEPR LUMA). C. Labrugère and P. Legros from PLACAMAT are acknowledged for XPS and SEM characterization studies. W. Z. acknowledges the China Scholarship Council for her visiting scholarship. C. L. is grateful for his visiting fellowship from the Shandong Government and Liaocheng University.

References

1 Q. Sun, Z. Ning, E. Yang, F. Yin, G. Wu, Y. Zhang and Y. Shen, Ligand-induced Assembly of Copper Nanoclusters with Enhanced Electrochemical Excitation and Radiative Transition for Electrochemiluminescence, *Angew. Chem., Int. Ed.*, 2023, **62**(44), e202312053.
2 W. Gu, H. Wang, L. Jiao, Y. Wu, Y. Chen, L. Hu, J. Gong, D. Du and C. Zhu, Single-Atom Iron Boosts Electrochemiluminescence, *Angew. Chem., Int. Ed.*, 2020, **59**(9), 3534–3538.
3 X. Gou, Z. Xing, C. Ma and J.-J. Zhu, A Close Look at Mechanism, Application, and Opportunities of Electrochemiluminescence Microscopy, *Chem. Biomed. Imaging*, 2023, **1**(5), 414–433.
4 A. Zanut, A. Fiorani, S. Canola, T. Saito, N. Ziebart, S. Rapino, S. Rebeccani, A. Barbon, T. Irie, H.-P. Josel, F. Negri, M. Marcaccio, M. Windfuhr, K. Imai, G. Valenti and F. Paolucci, Insights into the mechanism of coreactant electrochemiluminescence facilitating enhanced bioanalytical performance, *Nat. Commun.*, 2020, **11**(1), 2668.
5 M. Guo, D. Du, J. Wang, Y. Ma, D. Yang, M. A. Haghighatbin, J. Shu, W. Nie, R. Zhang, Z. Bian, L. Wang, Z. J. Smith and H. Cui, Three-Biomarker Joint Strategy for Early and Accurate Diagnosis of Acute Myocardial Infarction via a Multiplex Electrochemiluminescence Immunoarray Coupled with Robust Machine Learning, *Chem. Biomed. Imaging*, 2023, **1**(2), 179–185.
6 Y. Wang, S. Zhou, Y. Zheng, Y. Wang, Y. Hou, K. Wu, C. Huang, S. Liu, Y. Shen, R. Chen and Y. Zhang, Measurements of Local pH Gradients for Electrocatalysts in the Oxygen Evolution Reaction by Electrochemiluminescence, *J. Am. Chem. Soc.*, 2025, **147**(22), 19380–19390.
7 S. Knežević, D. Han, B. Liu, D. Jiang and N. Sojic, Electrochemiluminescence Microscopy, *Angew. Chem., Int. Ed.*, 2024, **63**(29), e202407588.
8 T. Sehar, G. Wei, Kainat, Zulqurnain, Iqra, R. Muhammad, F. Guo and L. Zhang, Recent Proceedings of Advanced Electrochemiluminescence Imaging Technology and Applications in Accurate Analysis, *Chem. Biomed. Imaging*, 2025, **4**(4), 485–509.
9 D. Han, B. Goudeau, D. Jiang, D. Fang and N. Sojic, Electrochemiluminescence Microscopy of Cells: Essential Role of Surface Regeneration, *Anal. Chem.*, 2021, **93**(3), 1652–1657.
10 S. Knezevic, L. Bouffier, B. Liu, D. Jiang and N. Sojic, Electrochemiluminescence microscopy: From single objects to living cells, *Curr. Opin. Electrochem.*, 2022, **35**, 101096.
11 Y. Wang, T. Liu, S. Yu, R. Luo, S. Bao, J. Wu, H. Ju, Z. Dai and J. Lei, Polychromatic Electrochemiluminescence Imaging of Single Heteroligand Metal–Organic Crystals, *Angew. Chem., Int. Ed.*, 2025, **64**(19), e202501151.
12 W. Zhao, H.-Y. Chen and J.-J. Xu, Electrogenerated chemiluminescence detection of single entities, *Chem. Sci.*, 2021, **12**(16), 5720–5736.
13 Y. Lu, X. Huang, S. Wang, B. Li and B. Liu, Nanoconfinement-Enhanced Electrochemiluminescence for *in situ* Imaging of Single Biomolecules, *ACS Nano*, 2023, **17**(4), 3809–3817.
14 Y. Liu, H. Zhang, B. Li, J. Liu, D. Jiang, B. Liu and N. Sojic, Single Biomolecule Imaging by Electrochemiluminescence, *J. Am. Chem. Soc.*, 2021, **143**(43), 17910–17914.
15 V. Gupta, F. Falciani, B. R. Layman, M. L. Hill, S. Rapino and J. E. Dick, Real-Time Visualization of Endogenous H_2O_2 Production in Mammalian Spheroids by Electrochemiluminescence, *Chem. Biomed. Imaging*, 2025, **3**(5), 310–321.
16 C. Mariani, A. Fracassa, P. Pastore, S. Bogialli, F. Paolucci, G. Valenti and A. Zanut, Singling Out the Electrochemiluminescence Profile in Microelectrode Arrays, *Chem. Biomed. Imaging*, 2025, **3**(7), 462–469.
17 Y. Chen, Y. Cao, C. Ma and J.-J. Zhu, Carbon-based dots for electrochemiluminescence sensing, *Mater. Chem. Front.*, 2020, **4**(2), 369–385.
18 R. Luo, D. Zhu, H. Ju and J. Lei, Reticular Electrochemiluminescence Nanoemitters: Structural Design and Enhancement Mechanism, *Acc. Chem. Res.*, 2023, **56**(14), 1920–1930.
19 T. Zhao, Q. Zhou, Y. Lv, D. Han, K. Wu, L. Zhao, Y. Shen, S. Liu and Y. Zhang, Ultrafast Condensation of Carbon Nitride on Electrodes with Exceptional Boosted Photocurrent and Electrochemiluminescence, *Angew. Chem., Int. Ed.*, 2020, **59**(3), 1139–1143.
20 S. Zhou, T. Zhou, Y. Hou, W. Li, Y. Shen, S. Liu, K. Wu and Y. Zhang, Recent advances in electrochemiluminescence based on polymeric luminophores, *Chin. Chem. Lett.*, 2025, **36**(5), 110284.
21 L. Xiang, Y. Hou, W. Li, K. Wu, K. Wang, Y. Wang, Y. Fang, S. Liu, Y. Shen and Y. Zhang, Boosting Electrochemiluminescence of Carbon Nitrides via Molecular Capacitor-Mediated Spatiotemporal Electron Coordination, *Adv. Sci.*, 2026, **13**(3), e06277.
22 R. Zhang, J. R. Adsetts, Y. Nie, X. Sun and Z. Ding, Electrochemiluminescence of nitrogen- and sulfur-doped graphene quantum dots, *Carbon*, 2018, **129**, 45–53.
23 L. Yang, C. R. De-Jager, J. R. Adsetts, K. Chu, K. Liu, C. Zhang and Z. Ding, Analyzing Near-Infrared Electrochemiluminescence of Graphene Quantum Dots in Aqueous Media, *Anal. Chem.*, 2021, **93**(36), 12409–12416.
24 E. Yang, H. Yang, Z. Ning, Y. Fang, M. Chen, Y. Zheng, W. Xu, G. Wu, Y. Zhang and Y. Shen, Construction of Carbon Dots with Wavelength-Tunable Electrochemiluminescence and Enhanced Efficiency, *Anal. Chem.*, 2022, **94**(47), 16510–16518.
25 J. Jin, X. Zhu, P. Zhou, H. Xie, X. Peng, Y. Chai and R. Yuan, Fe and Ni Dual-Atom Catalysts as High-Efficiency Coreaction Accelerators to Enhance the Electrochemiluminescence of the Carbon Dots/$S_2O_8^{2-}$ System for Assessing the Acute Myocardial Infarction Protein Marker, *Anal. Chem.*, 2025, **97**(43), 24105–24114.
26 C. Cheng, Y. Huang, X. Tian, B. Zheng, Y. Li, H. Yuan, D. Xiao, S. Xie and M. M. F. Choi, Electrogenerated Chemiluminescence Behavior of Graphite-like Carbon Nitride and Its Application in Selective Sensing Cu^{2+}, *Anal. Chem.*, 2012, **84**(11), 4754–4759.
27 J. Ji, J. Wen, Y. Shen, Y. Lv, Y. Chen, S. Liu, H. Ma and Y. Zhang, Simultaneous Noncovalent Modification and Exfoliation of 2D Carbon Nitride for Enhanced Electrochemiluminescent Biosensing, *J. Am. Chem. Soc.*, 2017, **139**(34), 11698–11701.
28 Y. Fang, H. Yang, Y. Hou, W. Li, Y. Shen, S. Liu and Y. Zhang, Timescale correlation of shallow trap states increases electrochemiluminescence efficiency in carbon nitrides, *Nat. Commun.*, 2024, **15**(1), 3597.
29 H. Zhang, J. Zhang, W. Chen, M. Tao, X. Meng, Y. Zhang and G. Zuo, Insight into structure evolution of carbon nitrides and its energy conversion as luminescence, *Carbon Energy*, 2024, **6**(2), e463.
30 Z. Wang, K. Wu, H. Yang, J. Cai, C. Wang, Y. Hou, S. Liu, Y. Shen, W. Wei, Y. Yang and Y. Zhang, Multi-color afterglow carbon nitrides via cascaded energy transfer, *Carbon*, 2026, **255**, 121555.
31 C. Zhao, C. Ma, S. Jia, M. Wang, M. Jiang, J. Ma, H. Yu and C. Hong, Ultrathin-N_2C-Deficient Carbon Nitride for Stabilized Enhancement of Electrochemiluminescence, *Small*, 2024, **20**(49), 2403138.
32 C. Zhao, C. Ma, M. Wang, W. Lai and C. Hong, Electrochemiluminescence Enhancement and Passivation Mitigation in Carbon Nitride Semiconductors *via* an Integrated Ternary Heterostructure Strategy, *Small*, 2024, **20**(26), 2310476.
33 R. Li, G. Yang, L. Zhao, X. Tan, R. Yuan and S. Chen, Vacancy Engineering of Nickel Single-Atom Catalysts to Enable Low-Triggering-Potential Electrochemiluminescence of Carbon Nitride, *Anal. Chem.*, 2025, **97**(37), 20127–20136.
34 L. Liu, Y. Liu, Y. Zhang, R. Yuan and H. Wang, K-Doped Graphitic Carbon Nitride with Obvious Less Electrode Passivation for Highly Stable Electrochemiluminescence and Its Sensitive Sensing Analysis of MicroRNA, *Anal. Chem.*, 2022, **94**(20), 7191–7199.
35 Y. Zhao, J. Descamps, Y. Léger, N. Sojic and G. Loget, Light Conversion by Electrochemiluminescence at Semiconductor Surfaces, *Acc. Chem. Res.*, 2024, **57**(15), 2144–2153.

36 Y. B. Vogel, N. Darwish and S. Ciampi, Spatiotemporal Control of Electrochemiluminescence Guided by a Visible Light Stimulus, *Cell Rep. Phys. Sci.*, 2020, **1**(7), 100107.
37 S. Han, H. J. Lee, T. Kim, S. Y. Lim and J. Kim, Flexible and Dynamic Light-Guided Electrochemiluminescence for Spatiotemporal Imaging of Photoelectrochemical Processes on Hematite, *Anal. Chem.*, 2024, **96**(28), 11146–11154.
38 M. Hwang, O. Bang and J. Kim, Light-guided patterning of electroactive PEDOT on hematite by utilizing spatially resolved photoelectrochemical processes in parallel, *Chem. Eng. J.*, 2025, **523**, 168284.
39 T. Kim and J. Kim, Light-Induced Chemiluminescence Microscopy for Imaging Heterogeneous Photo-Fenton-Type Activity on Individual Hematite Photocatalysts, *Angew. Chem., Int. Ed.*, 2025, **64**(49), e202509277.
40 Y. Zhao, J. Descamps, S. Ababou-Girard, J.-F. Bergamini, L. Santinacci, Y. Léger, N. Sojic and G. Loget, Metal-Insulator-Semiconductor Anodes for Ultrastable and Site-Selective Upconversion Photoinduced Electrochemiluminescence, *Angew. Chem., Int. Ed.*, 2022, **61**(20), e202201865.
41 J. Yu, H. Saada, R. Abdallah, G. Loget and N. Sojic, Luminescence Amplification at $BiVO_4$ Photoanodes by Photoinduced Electrochemiluminescence, *Angew. Chem., Int. Ed.*, 2020, **59**(35), 15157–15160.
42 J. Descamps, Y. Zhao, B. Goudeau, D. Manojlovic, G. Loget and N. Sojic, Infrared photoinduced electrochemiluminescence microscopy of single cells, *Chem. Sci.*, 2024, **15**(6), 2055–2061.
43 Y. Zhao, J. Descamps, Y. Léger, L. Santinacci, S. Zanna, N. Sojic and G. Loget, Upconversion photoinduced electrochemiluminescence of luminol-H_2O_2 at Si/SiO_x/Ni photoanodes, *Electrochim. Acta*, 2023, **444**, 142013.
44 Y. Zhao, J. Descamps, N. Al Hoda Al Bast, M. Duque, J. Esteve, B. Sepulveda, G. Loget and N. Sojic, All-Optical Electrochemiluminescence, *J. Am. Chem. Soc.*, 2023, **145**(31), 17420–17426.
45 J.-Y. Chen, C.-H. Xu and W. Zhao, Electrochemiluminescence and Photoinduced Electrochemiluminescence Probing of Energy Conversion Catalysis, *Chem. Biomed. Imaging*, 2026, DOI: 10.1021/cbmi.6c00028.
46 Y. Xiong, C.-H. Xu and W. Zhao, Photoinduced electrochemiluminescence: mechanistic insights and emerging applications, *Chem. Commun.*, 2026, **62**(26), 6865–6873.
47 Y. Zhao, B. Sépulveda, J. Descamps, F. Faye, M. Duque, J. Esteve, L. Santinacci, N. Sojic, G. Loget and Y. Léger, Near-IR Photoinduced Electrochemiluminescence Imaging with Structured Silicon Photoanodes, *ACS Appl. Mater. Interfaces*, 2024, **16**(9), 11722–11729.
48 L. Zhu, S.-J. Liu, Y.-H. Zhang, W. Chen, D. Zhu, R. Sun, P. Chen and Y.-Q. Lu, Light-Addressable Polychromatic Holographic Display *via* Multi-Encoded Chiral Superstructures, *Adv. Funct. Mater.*, 2025, **35**(47), 2507884.
49 I. M. Terrero Rodríguez, A. J. Borrill, K. J. Schaffer, J. B. Hernandez and G. D. O'Neil, Light-Addressable Electrochemical Sensing with Electrodeposited n-Silicon/Gold Nanoparticle Schottky Junctions, *Anal. Chem.*, 2020, **92**(16), 11444–11452.
50 C. Zhou, J. Descamps, B. Goudeau, P. Garrigue, F. Bedu, L. Santinacci, Z. Wang, N. Sojic and G. Loget, Photoelectrochemical Charge Transfer Imaging at Nanoscale Catalysts, *ACS Energy Lett.*, 2025, **10**(7), 3519–3525.
51 Y. Zhao, J. Yu, G. Xu, N. Sojic and G. Loget, Photoinduced Electrochemiluminescence at Silicon Electrodes in Water, *J. Am. Chem. Soc.*, 2019, **141**(33), 13013–13016.
52 Y. Zhao, J. Descamps, S. Ababou-Girard, J.-F. Bergamini, L. Santinacci, Y. Léger, N. Sojic and G. Loget, Metal-Insulator-Semiconductor Anodes for Ultrastable and Site-Selective Upconversion Photoinduced Electrochemiluminescence, *Angew. Chem., Int. Ed.*, 2022, **61**(20), e202201865.
53 K. Sun, S. Shen, Y. Liang, P. E. Burrows, S. S. Mao and D. Wang, Enabling Silicon for Solar–Fuel Production, *Chem. Rev.*, 2014, **114**(17), 8662–8719.
54 Z. Luo, T. Wang and J. Gong, Single-crystal silicon-based electrodes for unbiased solar water splitting: current status and prospects, *Chem. Soc. Rev.*, 2019, **48**(7), 2158–2181.
55 B. Fabre and G. Loget, Silicon Photoelectrodes Prepared by Low-Cost Wet Methods for Solar Photoelectrocatalysis, *Acc. Mater. Res.*, 2023, **4**(2), 133–142.
56 Y. Zhao, L. Bouffier, G. Xu, G. Loget and N. Sojic, Electrochemiluminescence with semiconductor (nano)materials, *Chem. Sci.*, 2022, **13**(9), 2528–2550.
57 D. Laser and A. J. Bard, Semiconductor electrodes. Photo-induced electrogenerated chemiluminescence and up-conversion at semiconductor electrodes, *Chem. Phys. Lett.*, 1975, **34**(3), 605–610.
58 J. Descamps, Y. Zhao, J. Yu, G. Xu, Y. Léger, G. Loget and N. Sojic, Anti-Stokes photoinduced electrochemiluminescence at a photocathode, *Chem. Commun.*, 2022, **58**(47), 6686–6688.